The Early-Cambrian Boho volcano of the El Graara massif, Morocco: petrology, geodynamic setting and coeval sedimentation.

José Javier Álvaro, H. Ezzouhairi, Emmanuelle Vennin, M.L. Ribeiro, Sébastien Clausen, A. Charif, N. Ait Ayad, M.E. Moreira

The Early-Cambrian Boho volcano of the El Graara massif, Morocco: Petrology, geodynamic setting and coeval sedimentation

J.J. Álvaro [a,b,*], H. Ezzouhairi [c], E. Vennin [d], M.L. Ribeiro [e], S. Clausen [b], A. Charif [c], N. Ait Ayad [c], M.E. Moreira [e]

[a] *Dpto. Ciencias de la Tierra, Universidad de Zaragoza, 50009 Zaragoza, Spain*
[b] *Laboratoire de Paléontologie et Paléogéographie du Paléozoïque, UMR 8014 CNRS, Université des Sciences et Technologies de Lille, 59655 Villeneuve d'Ascq, France*
[c] *Université Chouaib Doukkali, Département de Géologie, BP. 20, 24000 El Jadida, Morocco*
[d] *UMR 5561 CNRS, Biogéosciences, Université de Bourgogne, 6 bd. Gabriel, 21000 Dijon, France*
[e] *INETI—Area de Geocie^ncias, Estrada da Portela, Zambujal, 2721-866 Alfragide, Portugal*

A major volcanic episode is recorded across the Neoproterozoic-Cambrian transition in the Moroccan Anti-Atlas. Several volcanic cones are still preserved in the El Graara massif, laterally correlatable with volcanic flows dated as Early Cambrian (U/Pb date of 534 ± 10 Ma). Volcanic ashes and flows are interbedded with the uppermost part of the Adoudou dolostones, whereas the best-preserved volcano (the Boho Jbel) is onlapped by the overlying Lie-de-vin strata. Available petro-geochemical data from the Boho volcano suggest an alkaline magmatism probably derived from low-grade melting of a garnet–lherzolite mantle source, followed by fractional crystallization. The silica-undersaturated basaltic liquid evolved to form oversaturated rocks: the fractionation of a ferromagnesian phase with high-Ca and low-Al contents is suggested as the main process to cut across the critical plane of silica undersaturation in this geochemical series. Although the Boho geochemical patterns are similar to those of some rift emplacements, more data from other coeval magmatic eruptions are necessary to constrain their geodynamic setting.

Erosion of the Boho volcano favoured formation of a slope-apron composed of four sedimentary facies belts: chaotic megabreccia (related to downslope mass movements of rigid blocks), amalgamated breccia sheets (emplaced by viscous debris flows), a heterogeneous terrigenous belt (representing offshore substrates interrupted by channels intersected by cross-bedded shoals), and variegated shales and stromatolitic dolostones (typical of the Lie-de-vin Formation). Sharp changes in sedimentation rate were associated with modifications in paleorelief sloping and transport mechanisms from subaerial (?) rock fall at the foot of the cone escarpment to sheet-like debris flow on the slopes, and the replacement by sedimentation under wave and storm influence. The presence of an active carbonate productivity, recorded in the primary porosities of the Boho slope-apron, is suggested by widespread development of a robust, coelobiontic, microbial carbonate factory resilient to poisoning by terrigenous influx. Diagenesis in these deposits includes marine, meteoric and deep-burial cementation of calcite, dolomite, iron oxides, quartz, feldspar, and celestine, the latter indicating precipitation from hypersaline pore fluids.

Keywords: Alkaline basalts; Syenites; Slope apron; Diagenesis; Lower Cambrian; Morocco

* Corresponding author. Address: Dpto. Ciencias de la Tierra, University of Zaragoza, 50009 Zaragoza, Spain.
E-mail addresses: Jose-Javier.Alvaro@univ-lille1.fr (J.J. Álvaro), ezzouhairi_hassan@yahoo.fr (H. Ezzouhairi), emmanuelle.vennin@u-bourgogne.fr (E. Vennin), mluisa.ribeiro@ineti.pt (M.L. Ribeiro), Sebastien.Clausen@ed.univ-lille1.fr (S. Clausen), abdelcharif@hotmail.com (A. Charif), aitayad@hotmail.com (N.A. Ayad), eugenia.moreira@ineti.pt (M.E. Moreira).

1. Introduction

Subaerial volcanoes bearing steep escarpments are a major pathway for active erosion inducing a sedimentation on their flanks that form slope-apron settings commonly driven by gravity mass movements. As a result, the preservational potential of subaerial volcanoes is good under exceptional conditions associated with (i) sharp transgressive (marine) trends, (ii) subsequent active onlapping of slope-apron geometries burying and preserving the inherited volcanic paleotopography, and (iii) early-diagenetic cementation of the apron strata avoiding their reworking.

The Alougoum volcanic complex located on the western El Graara massif (Fig. 1) contains one of the best-preserved volcanoes emplaced in the Lower Cambrian of Morocco. The knoll-shaped edifice of the Boho Jbel (previously reported by Choubert, 1952; Boudda et al., 1979; Destombes et al., 1985; Buggisch and Flügel, 1988; among others) is still observable rising from the oueds and plains of the El Graara massif. Its preservation was directly related to rapid burial and isolation from later erosion made up by a thick, concentrically surrounding slope-apron. The multidisciplinary aims of this paper are (i) to document the available mineralogical and geochemical data that contribute to its petrological interpretation, (ii) to characterize the modifications in sedimentary architecture of its onlapping slope-apron, and (iii) to understand the polyphasic cementation processes that took place in the slope-apron intergranular porosities stabilizing the volcanic paleotopography.

2. Geologic setting and stratigraphic framework

The Neoproterozoic-Cambrian transition is recognized in the Moroccan Anti-Atlas throughout a carbonate-dominated succession (Adoudou and Lie-de-vin formations; Choubert, 1952, 1953a,b) that unconformably overlies (via a post-Pan-African unconformity) the Ouarzazate Group (Fig. 2). This time span is characterized in the region by an episodic volcanic activity, mainly reported as volcaniclastic tuffs, andesites and ignimbrites. The ignimbrites of the upper part of the 'Série d'Ouarzazate'or Ouarzazate Group have yielded Late Neoproterozoic (ca. 586–563 Ma) or Precambrian III, U/Pb volcanic zircon and Rb/Sr whole-rock ages (Clauer et al., 1982; Mifdal and Peucat, 1985).

Volcanic ashes and flows also occur interbedded with the Adoudou and Lie-de-vin strata (Choubert and Faure-Muret, 1970). One source for these ashes is preserved in the Alougoum volcanic complex located on the El-Gloa (El-Gleuh) area (Choubert, 1952; Boudda et al., 1979, Fig. 1), in which volcanic paleotopographies cover directly the Adoudou dolostones and were progressively onlapped

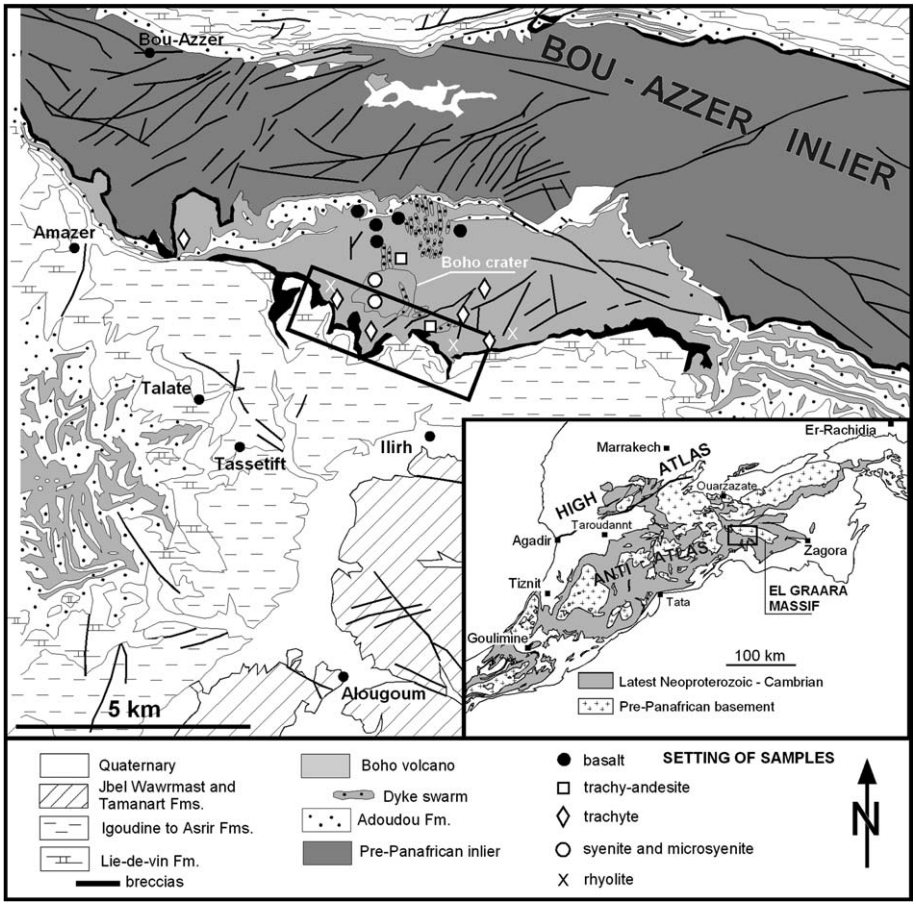

Fig. 1. Geologic setting of the Boho volcano in the western El Graara massif (modified from SGM, 1970) showing sampling location.

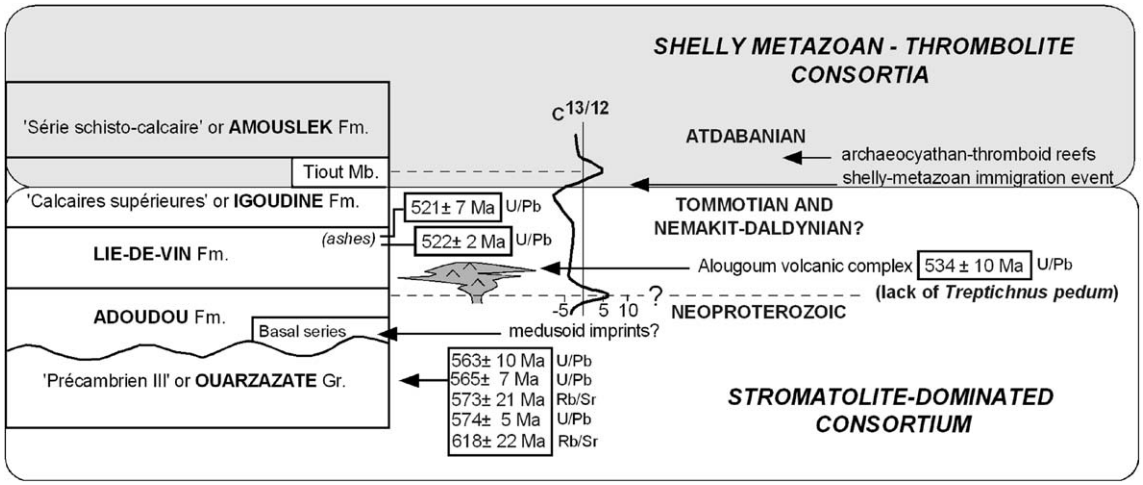

Fig. 2. Lithostratigraphic units of the Neoproterozoic-Cambrian transition in the Moroccan Atlas with the chronologic succession of event stratigraphy (summarized after Ducrot and Lancelot, 1977; Houzay, 1979; Leblanc and Lancelot, 1980; Clauer et al., 1982; Destombes et al., 1985; Tucker, 1986; Kirshvink et al., 1991; Latham and Riding, 1990; Magaritz et al., 1991; Compston et al., 1992; Debrenne and Debrenne, 1995; Geyer et al., 1995; Landing et al., 1998; Walsh et al., 2002).

by the breccias, dolostones, variegated shales and sandstones of the Lie-de-vin Formation. An early U/Pb date of 534 ± 10 Ma from the Boho volcano (Ducrot and Lancelot, 1977) suggests that deposition of the uppermost part of the Adoudou Formation took place in the pre-trilobite earliest Cambrian. As a result, the location of the Neoproterozoic-Cambrian boundary (defined by the first appearance of the ichnospecies *Treptichnus* (former *Phycodes*) *pedum*; Narbonne et al., 1987) remains problematical in Morocco because it lies within the thick carbonate-dominated Adoudou Formation, extremely poor in shelly metazoans and ichnofossils. The boundary has been tentatively correlated with carbon isotope signatures (Tucker, 1986; Latham and Riding, 1990; Kirshvink et al., 1991; Magaritz et al., 1991) above the medusoid-like imprints of the 'Série de base' or Basal series (Adoudou Formation; Houzay, 1979) and below the occurrence of Atdabanian (*sensu* Spizharski et al., 1986), shelly metazoan fossils in the Tiout Member (Sdzuy, 1978; Monninger, 1979; Schmitt, 1979; Debrenne and Debrenne, 1995, see Fig. 2).

3. The Boho volcano emplacement: mineralogical and geochemical features

The Boho volcano (Fig. 1) is elliptic in outline (ca. 6 × 22 km), and forms a topographic high of ca. 300 m with a crater relic of ca. 2 km in diameter. The cone was intruded by a swarm of N–S-trending dykes that strengthened the framework. Eruptive products likely expelled explosively as the volcano profile is still steep, and intercalation of lavas and pyroclastic tuffs occur both on the northern and southern volcano flanks, giving rise to a (polygenic) stratovolcano that recorded repeated episodes of volcanic activity, each characterized by different petrographic types. The lack of pillow-lava structures and thin films of small vesicles paralleling the lava flows suggest subaerial exposure to shallow-water emplacement conditions.

From a petrologic point of view, the Boho volcano consists of a syenitic-trachytic core surrounded by a great variety of volcanic rocks, which are essentially of basaltic composition in the northern flank and trachytic-rhyolitic with associated pyroclastic tuffs and breccias in the southern flank. The basalts are interstratified with the Adoudou dolostones, as pointed out by Choubert (1952) and Leblanc (1973). A swarm of metre-thick, N–S-trending dykes of microsyenites, trachyandesites and trachytes cross cut the volcano.

The syenites of the inner core are pink-coloured, medium-grained, porphyritic rocks. Prominent phenocrysts ($\leqslant$4 mm) are made up of K-feldspar and plagioclase, and a few crystals of aegirine–augite clinopyroxene surrounded by hornblende, and biotite. The groundmass is rich in K-feldspar, biotite and iron oxides. Apatite is the most common accessory mineral in these rocks (Fig. 3A). The syenitic core is surrounded by porphyritic microsyenites with large laths ($\leqslant$6 mm) of K-feldspar, plagioclase and femic minerals intensely transformed into a secondary mineral association of albite, chlorite, hematite and epidote (Fig. 3B). The groundmass consists of fine-grained K-feldspar, plagioclase, iron oxide and apatite associated with epidote and chlorite.

The basalts that crop out essentially on the northern side of the Boho volcano correspond to thick lava flows. The porphyritic textures display micro-phenocrysts ($\leqslant$1.5 mm) of plagioclase and femic minerals completely retromorphosed to chlorite, epidote, calcite and iron oxides. The groundmass consists of feldspar microlithes with intergranular clinopyroxene and iron oxides (Fig. 3C).

The trachyandesites crop out mainly in the southern and central parts of the massif. The textures are porphyritic with plagioclase and clinopyroxene phenocrysts surrounded by a groundmass containing the same minerals and iron oxides as millimetre-sized crystals. Rare, tiny quartz grains are sometimes present in the groundmass (Fig. 3E).

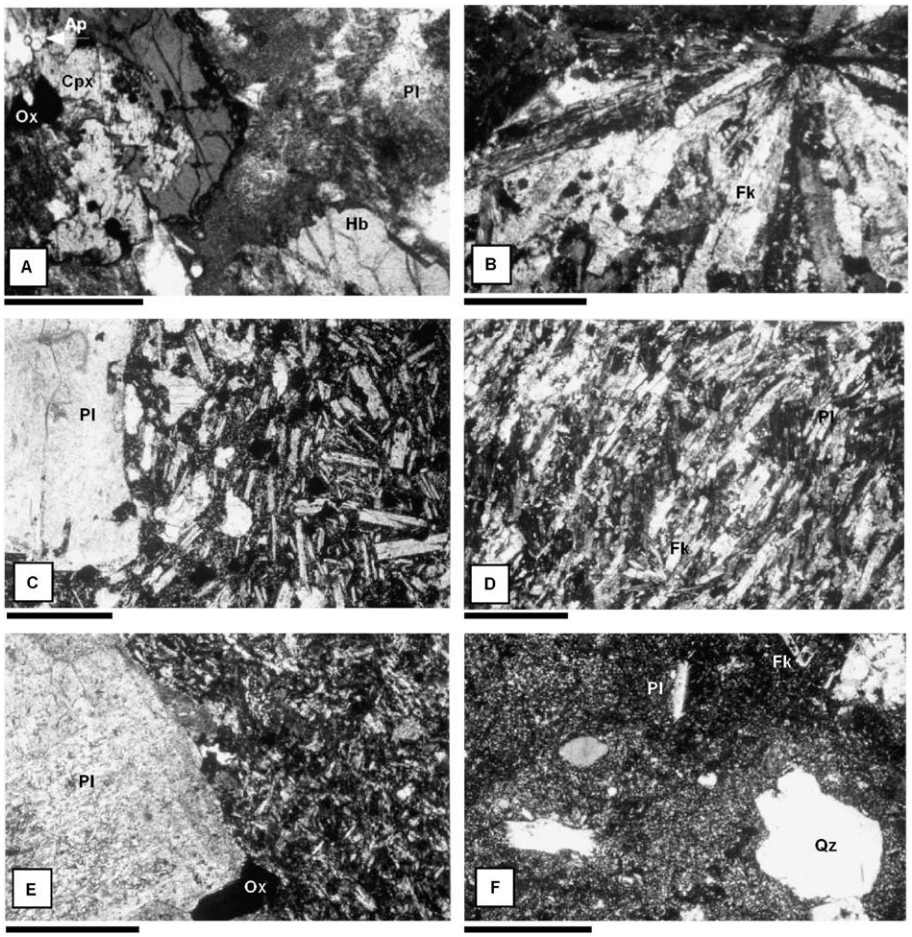

Fig. 3. Thin-section photomicrographs of the volcanic rocks described in the text. (A) Inner-core medium-grained syenite with clinopyroxene crystals surrounded by hornblendes (normal light). (B) Microsyenite with radial distribution of feldspars (polarized light). (C) Basalt with porphyritic texture (n.l.). (D) Trachyte with fluidal texture due to preferred orientation of alkaline feldspar laths (p.l.). (E) Trachyandesite with porphyritic texture (p.l.). (F) Rhyolite with partly resolved quartz phenocrysts in a fine felsitic groundmass (p.l.). Scales: A = 1 mm, B–E = 2 mm, C = 0.5 mm, D = 1.5 mm, F = 0.6 mm. Ap, apatite; Cpx, clinopyroxene Fk, potassium feldspar; Hb, hornblende; Ox, iron oxide; Pl, plagioclase; Qz, quartz.

The trachytes usually display fluidal microlithic textures, locally porphyritic (Fig. 3D). The phenocrysts ($\leqslant$1.5 mm) are of plagioclase and K-feldspar, the latter commonly retromorphosed to chlorite, epidote and calcite. The millimetre-sized, fluidal feldspar microlithes of the groundmass contain intergranular quartz and iron-oxide grains.

The rhyolites crop out essentially in the southern part of the massif. Phenocrysts of corroded quartz and Na- and K-feldspars ($\leqslant$1 mm) are surrounded by a fine-grained felsitic groundmass (Fig. 3F).

The geochemical data are based on 18 chemical analyses of representative samples (Table 1). The geochemical data of the major and trace elements were analysed by X-ray fluorescence at the INETI laboratory in Porto, Portugal. Precisions for major and trace elements are usually better than 2% and 5–10%, respectively. As the selected samples show only incipient alteration of primary mineralogy, we consider that the analyses represent their igneous geochemistry. In spite of some scattering of the data, due to some major element mobility related to supergenic alteration and volatile transfer, the total alkalis vs. silica projection displays an alkaline trend from basalt and trachyandesite to trachyte-rhyolite types (Fig. 4). The Mg# ratios are respectively 0.44 for the basalts, 0.07 for the trachyandesites, and 13 for the rhyolites. These ratios indicate strong fractionation of the chemical elements from the basic to the acidic terms of the sequence. The broadly linear trends in the Nb vs. Zr and Y vs. Zr diagrams suggest that the rocks derived from the same mantle source, and mostly evolved by fractional crystallization, with the exception of the two most silicic samples, which do not plot on the same line (Fig. 5). The Harker diagrams suggest olivine, clinopyroxene, amphibole, plagioclase and iron-oxide fractionation.

The final oversaturated rock types in the alkaline and alkaline-transitional series are usually explained by the effect of a combination of two processes: (i) crustal contamination of the originally undersaturated liquid and (ii) fractional crystallization. The first hypothesis cannot be confirmed due to the lack of isotopic data. However, based on geochemical data (Fig. 5), we can infer that fractionation was the major geochemical process.

Table 1
Average chemical composition in major (%) and trace (ppm) elements of the earliest-Cambrian Boho rock types; standard deviation in parentheses when $n > 3$

	Basalt		Trachy-andesite	Syenite/ microsyenite	Trachyte		Rhyolite
n	5		2	2	6		3
SiO_2	45.08	(1.70)	50.88	62.78	64.61	(1.30)	68.57
Al_2O_3	15.46	(0.79)	15.99	16.31	15.04	(1.24)	14.62
Fe_2O_3[a]	12.32	(1.83)	12.07	5.43	7.69	(2.21)	4.12
MnO	0.11	(0.06)	0.11	0.20	0.05	(0.01)	0.04
CaO	5.33	(1.06)	4.95	2.06	0.71	(0.80)	1.26
MgO	9.09	(3.02)	1.86	0.67	1.69	(1.31)	1.16
Na_2O	2.09	(1.58)	5.34	4.78	3.26	(1.82)	2.93
K_2O	2.83	(1.26)	2.86	5.27	4.87	(1.81)	5.35
TiO_2	2.96	(0.12)	2.44	0.83	0.45	(0.09)	0.31
P_2O_5	0.64	(0.21)	0.57	0.20	0.05	(0.03)	0.02
LOI	3.69	(0.73)	2.52	1.10	1.22	(0.46)	1.32
Total	99.60		99.58	99.62	99.65		99.71
Rb	33	(10)	55	105	93	(45)	125
Sr	130	(56)	141	78	18	(5)	17
Y	23	(6)	37	52	60	(8)	101
Zr	210	(89)	328	524	738	(148)	1593
Nb	39	(49)	64	85	117	(25)	182
Ba	641	(418)	530	605	309	(145)	252
Ta	6	(4)	4	5	7	(4)	2
Th	15	(13)	11	13	20	(10)	7
Hf	17	(13)	12	11	20	(12)	6
Yb	7	(4)	5	5	6	(4)	3

n = number of samples in population; LOI = loss on ignition.
[a] Total iron as Fe_2O_3.

This kind of geochemical evolution is usually associated with rift zones. The spiderdiagrams (Fig. 6) display a similarity between the Boho alkali basalts and other alkali basalts from continental rift zones. However, the Boho volcano represents only a single magmatic episode and, to determine its geochemical affinity, further information from other volcanic rocks of the whole Alougoum volcanic complex seems necessary. Other comparable alkaline volcanic rocks are also known from the Middle Cambrian of Ben Maachou (Moroccan Coastal Block), although tholeiites were recorded in the Lower Cambrian of Azegour (High Atlas) and the western Anti-Atlas (Ezzouhairi et al., 2003; Ait Ayad et al., 1998; Soulaimani et al., 2003). The magmatism of the High Atlas has already been compared with those of the same age from the southern Iberian Peninsula, which represents an aborted continental rift (Mata and Munha, 1990; Ait Ayad et al., 1998). The western Anti-Atlas magmatism was interpreted as settled in a continental extensional environment. In our opinion, an extensional geodynamic setting, such as a continental rifting, could fit well with the emplacement of the Boho volcano; however, further data from other coeval volcanic activities are necessary to constrain it.

The alkaline magmatism associated with the emplacement of the Boho volcano is key to understand the evolution of the geodynamic activity in the Moroccan margin of Gondwana across the Neoproterozoic-Cambrian transition. This transition has recorded a distinct evolution of the igneous activity from calc-alkaline to alkaline intra-plate and/or continental tholeiitic volcanism (Ezzouhairi, 2001). This magmatic evolution reflects a tectonic inversion from a Neoproterozic (Pan-African) compressive margin (Badra et al., 1992; Jouhari et al., 2001; Ouazzani, 2001) to intra-plate extension related to latest Neoproteorozic-early Cambrian rifting processes (Piqué et al., 1995). As envisaged by Ezzouhairi (2001) and El Archi et al. (2004), this major geodynamic modification from 'orogenic' to 'anorogenic' geodynamic episodes started earlier (latest Neoproterozoic) in the Anti-Atlas, reached the western High Atlas after the earliest Cambrian (Badra et al., 1992; Ait Ayad et al., 1998), and occurred even later in the Meseta domains (Ouali et al., 2000, 2003; Ribeiro et al., 2001; El Attari, 2001).

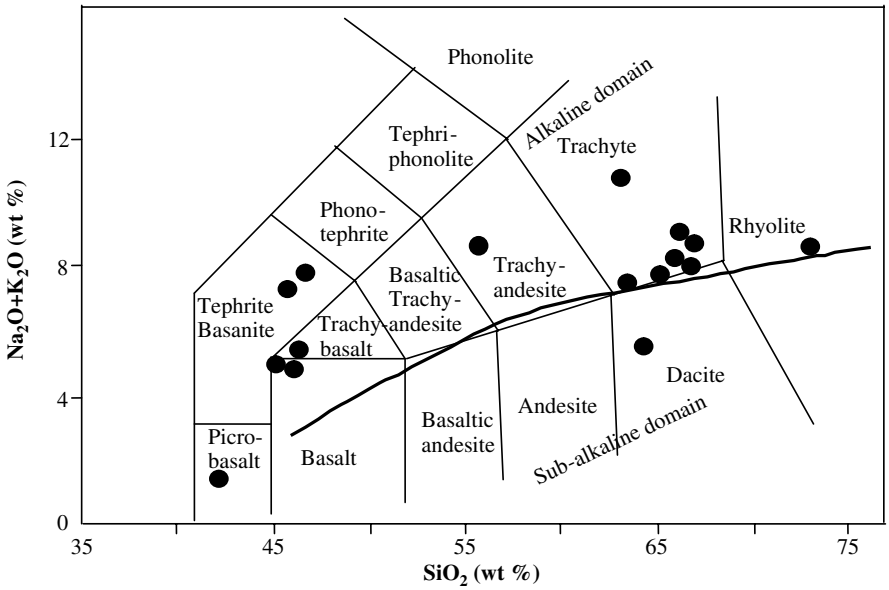

Fig. 4. Total alkalis vs. silica diagram for the Boho volcanic rocks; TAS, diagram after LeBas et al. (1986); the alkaline/sub-alkaline boundary is from Kuno (1966).

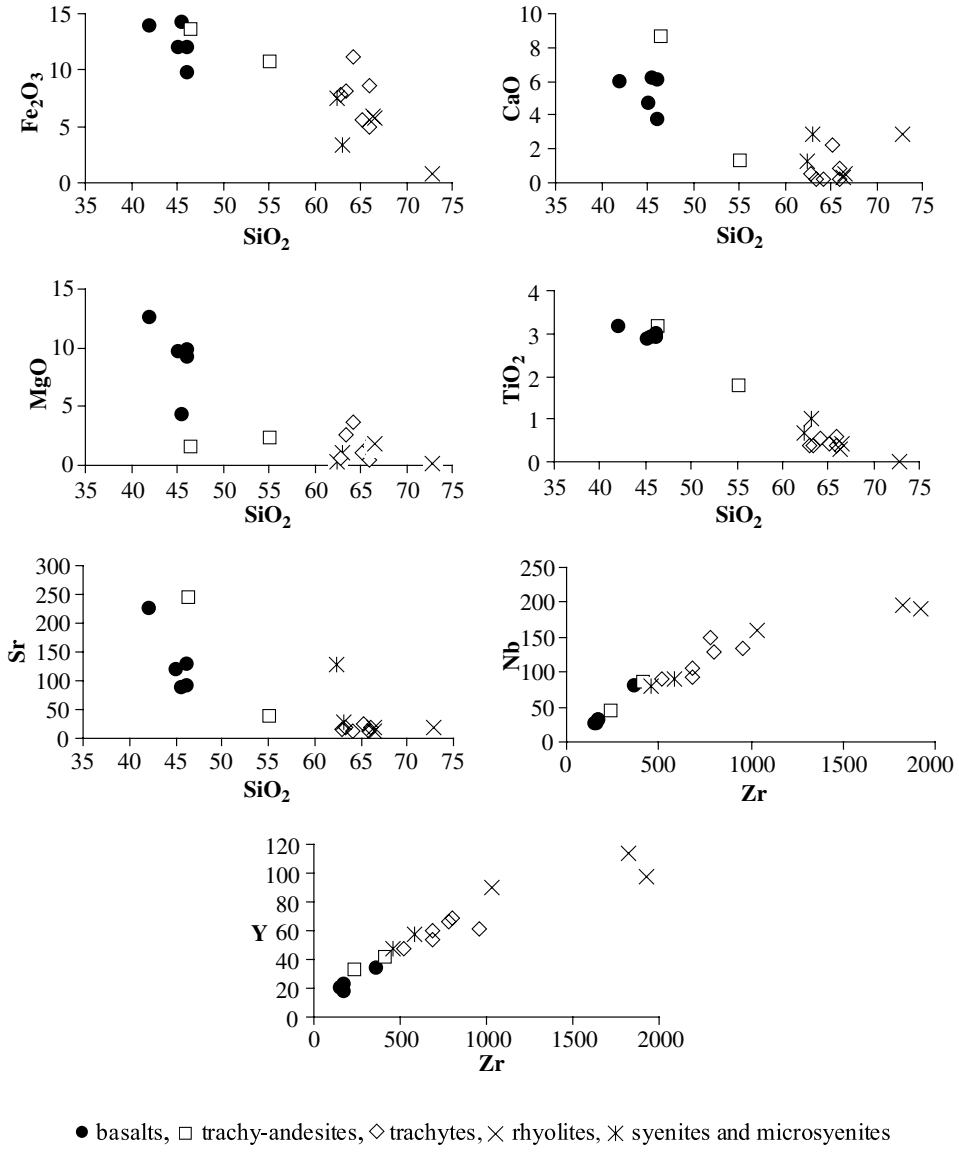

Fig. 5. Variation of Fe_2O_3, CaO, MgO and TiO_2 vs. SiO_2, and Nb and Y vs. Zr for the Boho volcanic rocks; major elements in % and trace elements in ppm.

4. Sedimentary belts of the onlapping slope-apron

Once the eruptive activity ceased, the volcano became a passive source of erosion. It shed enough volcaniclastic material to form a prominent clastic wedge sedimented in a centrifugal pattern. The preserved volcanic margins of the uppermost high-steep escarpments (up to 50° in relief) change downwards into a highly eroded low-relief margin (slope less than 20°). Major canyons that would capture large volumes of sediment and funnel them into the flat seafloor are absent. The slope-apron sedimentary rocks change laterally into the classical Lie-de-vin Formation composed of purple and reddish claystones, stromatolitic dolostones and sandstones. Four sedimentary facies associations occur in a regular concentric pattern with belt boundaries running parallel to the margin of the Boho volcano (Fig. 7). The identification and lateral distribution of the facies belts are reported in this paper from a radial down-slope transect located at the southwestern edge of the volcano (Figs. 1 and 8A).

4.1. Chaotic megabreccia

This massive, clast-supported, polymictic breccia directly overlies the flanks of the Boho volcano (Fig. 8B–D). Its thickness ranges from 1 to at least 30 m, increasing in a radial pattern, although its greatest thickness is not measurable due to the partial cover made by oued-related deposits. The breccia is mostly composed of centimetre- to metre-scale volcaniclastic clasts and blocks (up to 1.6 m long). The clasts, poorly sorted, are angular to subangular in shape. Grading is absent and distinct sheets, channels or bedding are not developed. Blocks are neither folded nor contorted, and are randomly oriented. Matrix

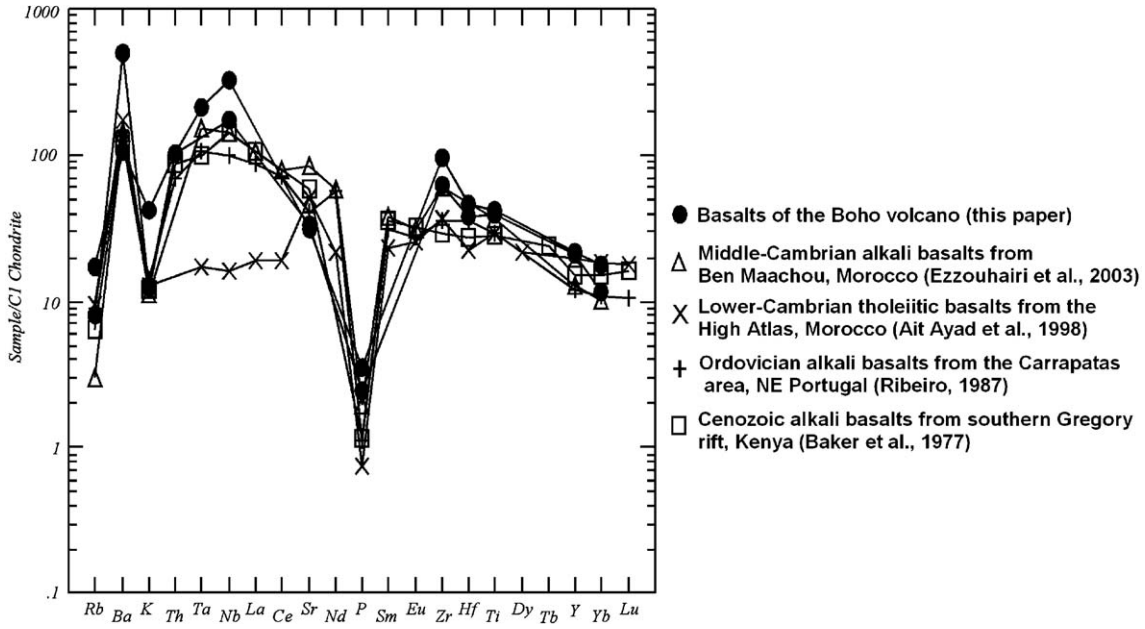

Fig. 6. Chondrite C1 (Sun and McDonough, 1989) normalised trace-element patterns for representative basalts from the Boho volcano compared to Lower-Cambrian tholeiitic basalts from the High Atlas, Middle-Cambrian alkali basalts from Ben Maachou (Morocco), Ordovician alkali basalt from NE Portugal, and Cenozoic alkali basalts from southern Gregory Rift (Kenya); modified from Ait Ayad et al. (1998), Baker et al. (1977), Ezzouhairi et al. (2003), and Ribeiro (1987).

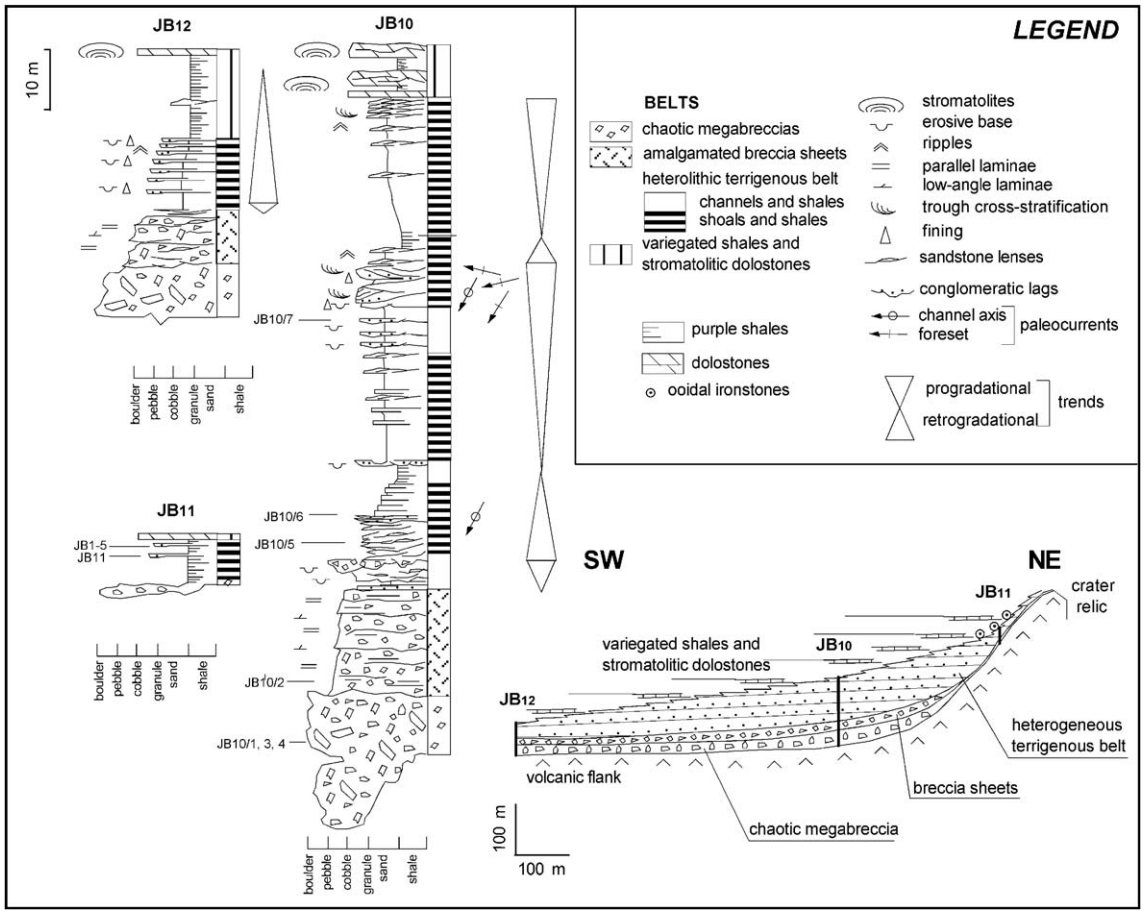

Fig. 7. Stratigraphic logs of the southern Boho slope-apron and reconstruction of the southwestern edge of the volcano flank.

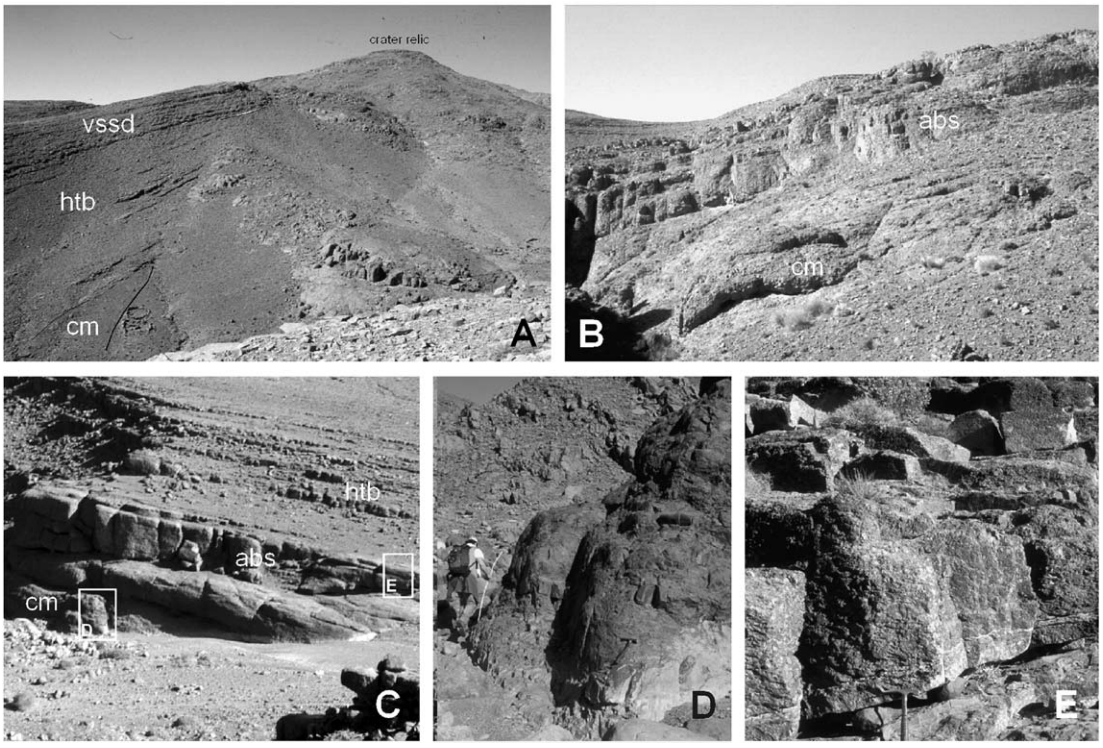

Fig. 8. Field aspect of the Boho slope-apron deposits. (A) Lateral view of onlapping patterns with three facies belts, and setting of section JB_{11}. (B) Frontal view of onlapping patterns with both breccia-dominated belts and setting of section JB_{10}. (C) Setting of section JB_{12} with details of chaotic megabreccia (D) and breccia sheets (E); cm—chaotic megabreccia; abs—amalgamated breccia sheets; htb—heterolithic terrigenous belt; vssd—variegated shales and stromatolitic dolostones.

composition consists of an unsorted mixture of quartz, feldspar and volcanigenic, coarse-grained sand to silt and terrigenous clay in variable proportions.

Deposition of the chaotic breccia was directly related to large- and small-scale downslope mass movements of rigid rocks, such as rock fall and subordinate rolling and slides of individual blocks or clasts along gliding surfaces indicating lack of block rotation (slumping) during transport and deposition. The lack of internal sedimentary structures does not allow identification of coeval debris-flow processes. Thickness variations are mainly related to the infill of an irregular, inherited paleotopography.

4.2. Amalgamated breccia sheets

They form decimetre- to metre-scale, tabular to sheet bodies, bounded by sharp, planar and slightly scoured contacts but lacking distinct channel-like structures (Figs. 8B–E). The lowermost part of each sheet is clast-supported and inversely graded, whereas its upper part (up to 30 cm thick) shows normal grading from clast- to matrix-supported, boulder to granule breccias and conglomerates, and coarse-grained sandstones. Breccia contains polymictic clasts, up to 30 cm in size, subrounded to angular in shape, with a predominance of basalt, syenites and trachytes. Matrix can be siliciclastic and secondarily calcarenitic (with a patchy distribution). The clast/matrix ratio is variable, with the clast percentage ranging between 40% and 80%. Clasts are locally imbricated or define a planar cross bedding. The vertical amalgamation of the individual fining-upward sheets is arranged into a thinning- and fining-upward trend related to a coeval change from clast- to matrix-supported fabric.

The presence of poor sorting, polymodal clast size, subhorizontal orientation of the long axes of clasts, grading and imbrication, and the lack of distinct basal channels, all indicate that these sheets are debrites emplaced by viscous debris flows (poorly sorted debris only requires a small percentage of primary mud matrix, around 5% for large-slope collapse debris; Einsele, 1991; Valladares, 1995). The sandy-matrix content suggests that deposition occurred from sandy debris-flows, later reworked by traction, beneath a high-concentration turbidity regime. The gradual transition between breccias to sandstones suggests that these flows changed gradually from debris flows (involving deposit of the coarsest load by mass emplacement) to sandy high-density turbidity currents.

4.3. Heterolithic terrigenous belt

This belt directly overlies the above-described breccia belts (Fig. 8A), in which two distinct facies associations are recognized and described below:

(a) Alternations of isolated to amalgamated channels and shales. This facies association, up to 2 m thick, displays lenticular bodies with channeled lower contacts that are

broadly concave-upwards. Each channel is 1–4 m wide and up to 2 m thick. They are lined with lag concentrations, less than 20 cm thick, of clast-supported, angular to subangular, polymictic granule to gravel breccia grading upwards into medium-sorted, medium- to very-coarse grained litharenites (bearing soft siltstone to sandstone clasts with carbonate cement patches). Channel-fill structures are dominated by stacked, fining trends of small-scale (each of them up to 80 cm thick), through and planar cross-stratified sets with local low-angle lamination and topped by asymmetric and symmetric ripples. Paleocurrents of channel axes range from SSW to SW (200–230°). Channels are encased in structureless greenish shales, up to 12 m thick.

The granule to litharenite sandstones were deposited as channels filled by intersected cross-bedded sets. The unimodal character of the paleocurrent indicators indicates that these sandstones were not deposited as meandering, but as linear-dominated subtidal channel systems, likely related to the slope of the volcanic flank.

(b) Alternations of sandstone shoals and shales. This association occurs as 4–30 m thick units, and is characterized by alternations of very coarse- to very fine-grained sandstones and shales. The former consist of moderately sorted litharenites and lithic greywackes rich in calcarenitic and polyphasic volcanigenic clasts, some of them bearing patches of carbonate microsparitic cements, irregularly distributed, which can reach locally more than 50% in volume. Sandstone beds and lenses, up to 2.2 m thick, display trough cross-laminae, wave-rippled and low-angle laminae arranged in medium-scale sets with irregular reactivation surfaces and foreset dips from 20° to 30°. Erosive contacts and gutter casts are commonly observed at the base of the beds. Basal lags consist of soft, rip-up, shale and polyphasic volcanigenic clasts covering the lowermost 20 cm of some beds. Paleocurrent measurements were obtained from three-dimensional exposures of trough cross-laminated sandstones, where foreset progradations range from W to SE. The shale alternations consist of siltstones and green and purple claystones, with subordinate fine- and medium-grained sandstones. Siltstones contain centimetre-thick, medium-grained sandstone intercalations exhibiting erosive bases, and grading. They lack good stratification, as suggested by millimetre-thick, finely crinkled, sandy laminae. As a whole, the sandstone/shale alternations are incorporated into both thickening- and coarsening-upward trends and thinning- and fining-upwards trends, up to 35 m thick (see Fig. 3).

Individual beds represent the succession of stacked, polydirectional downstream, migrating megaripple bedforms, as indicated by their polymodal paleocurrent distribution pattern. The multiprovenance and angularity of intraclasts and fining-upward fills provide some clues regarding the dynamics of the shoals, as they indicate episodic rather than continuous activation and fill. The shale alternations were probably deposited on offshore substrates, under essential calm-water conditions as evidenced by the dominance of siliciclastic mud, in which the interbedded siltstone and fine-grained sandstone beds were probably related to storm surges. The occurrence of calcarenitic clasts, which increase in abundance towards the top of the coarsening-upward trends suggest late reworking of previous slope-apron deposits bearing carbonate cements: this indicates short-distance transport and 'cannibalism' (storage and subsequent reworking) of proximal deposits. The mechanisms proposed for the generation of the above-described trends are analogous to that of siliciclastic platform progradations and retrogradations related to fluctuations in terrigenous input and relative sea level.

4.4. Variegated shales and stromatolitic dolostones

This facies association represents the typical Lie-de-vin sedimentary rocks and occurs, for the first time, 30 m above the lowermost-preserved slope-apron (so that featuring the Adoudou/Lie-de-vin contact; Fig. 8A). The lowermost part of the Lie-de-vin Formation is dominated by purple-to-reddish shales bearing episodic yellowish dolostone beds (up to 50 cm thick) and, scarce, centimetre-scale sandstone intercalations (representing the above-described facies association 4.3 b). The bulk of the dolostones consists of crinkled stromatolites that, in some examples, accrete vertically into dome-shaped stromatolites, up to 1 m in diameter.

The rarity of sedimentary structures and the lateral disappearance of sandstones (passing into stromatolitic dolostones) do not allow us to propose a definitive environmental interpretation, although bottom energy is only locally preserved in the form of centimetre-thick shoals. The lack of shelly and burrowing fauna, and the episodic growth of microbial mats indicate sedimentation in a subtidal (lacking subaerial-exposure structures) setting, only ecologically favourable to stromatolitic growth.

5. Diagenetic cementation and associated carbonate productivity

Interpretation of cementation history was made by distinguishing cement types based on colour, brightness, luminescence patterns, iron content, cement morphology, and crosscut relationships (summarized in Fig. 9). Complex

Fig. 9. Idealized diagenetic succession affecting the slope-apron deposits in logs JB_{10} and JB_{11} (from eogenesis to telogenesis). (A) Early to late diagenesis affecting a thrombolitic boundstone with ooidal-packstone matrix (JB_{11}). (B) Late diagenetic cementation and dissolution of pores (JB_{10}). (C) Late diagenetic phases (JB_{10} and JB_{11}) affecting all the previous cementation and dissolution episodes and (D) Sketches of Fig. 10A, 10I, 10H, and 10G; * saddle *sensu* Radke and Mathis (1980), ** baroque *sensu* Zenger (1983) with curved faces, undulose extinction and irregular intercrystalline contacts typical of replacive forms (Gawthorpe, 1987), and *** similar to those known in quartz and other silicates (Kastner, 1971).

(A) FIRST DIAGENETIC DOMAIN

mineral cement	occluded porosity	shape	luminescence	size	fig. 10
1, celestine	intergranular pores	equant, euhedral	nonluminiscent	1000-2500 µm	A-B
SOLUTION (dis-0)					
2, calcite core and dolomite rim — 2a, dolomite (d2)	remaining intergranular pores + mm-sized solution vugs	1st rims and internal crystal vugs	reddish	100-250 µm	
SOLUTION (dis-1) — ***DEDOLOMITIZATION*** (dd-1)					
2, calcite core and dolomite rim — 2b, calcite	core and embayed contacts	irregular	dull orange (crystal cores)	125-2000 µm	B
SOLUTION (dis-2) — ***DEDOLOMITIZATION*** (dd-2)					B
3a, calcite	solution vugs and embayed core+1st rim contacts	euhedral	dull	100-500 µm	
3b, iron-rich calcite	embayed and irregularly truncated core+1st rim/2nd rim contacts	2nd rim/subhedral	bright yellow	250-500 µm	
SOLUTION (dis-3)					
3c, calcite	vugs crosscutting celestine+dolomite cements	blocky	dull	up to 1 cm	

(B) SECOND DIAGENETIC DOMAIN

1, calcite (microsparite to sparite)	intergranular pores / replacing marine fibrous crystals and coating ooids and clasts	- equant to drusy - prismatic	- dull - bright yellow	10-50 µm 50-75 µm	H
2a, mimetic dolomite	replacing prismatic calcite	prismatic	bright orange to reddish	50-75 µm	
2b, dolomite (d1)	- replacing euhedral dolomite	anhedral & unzoned: xenotopic mosaics (d1a)	reddish to orange in core and dull to nonluminiscent in margins	100-250 µm	F
	- lining pore walls	anhedral & unzoned: idiotopic mosaics, euhedral rhombs (d1b)		25-125 µm	
SOLUTION					
2c, dolomite	irregular and embayed outlines of cores and margins	saddle* or baroque ** hypidiotopic to xenotopic replacive forms	dull orange	500-5000 µm	G-H
3a, calcite	remaining pores	blocky	dull	up to 1000 µm	
DEVELOPMENT OF VEINS AND FISSURES					
3b, calcite	lining tectonic veins and fissures	drusy	- bright yellow - patchy dark when associated with iron concentrations	25-125 µm	
4, celestine	replacing and corroding calcite vein-filling cements	euhedral	nonluminiscent	250-1000 µm	

(C) LATE DIAGENESIS

1, feldspar	- skeletal moulds - veins - vugs	euhedral fibrous rims subhedral (drusy)	nonluminiscent to dark + blue emission related to structural defects***	25-60 µm	H I
2, clays	along cleavage heterogeneities and bordering secondary vugs	fibrous	dark	5-10 µm	
DEVELOPMENT OF VEINS AND FISSURES					
3, quartz	remaining porosity and veins	isopachous drusy mosaics	dark blue	150-500 µm	I
4, iron oxi-hydroxide pyrite + deerite	crosscutting previous silica crystals	euhedral fibrous	dark	500-700 µm (long axes)	
DEVELOPMENT OF VEINS AND FISSURES					
5, calcite	remaining pores	blocky	homogeneous dull	50-100 µm	G-I
DEVELOPMENT OF VEINS AND FISSURES					
6, calcite	lining the latest vein network	drusy	bright yelllow	50-75 µm	

(D) CROSSCUTTING RELATIONSHIPS

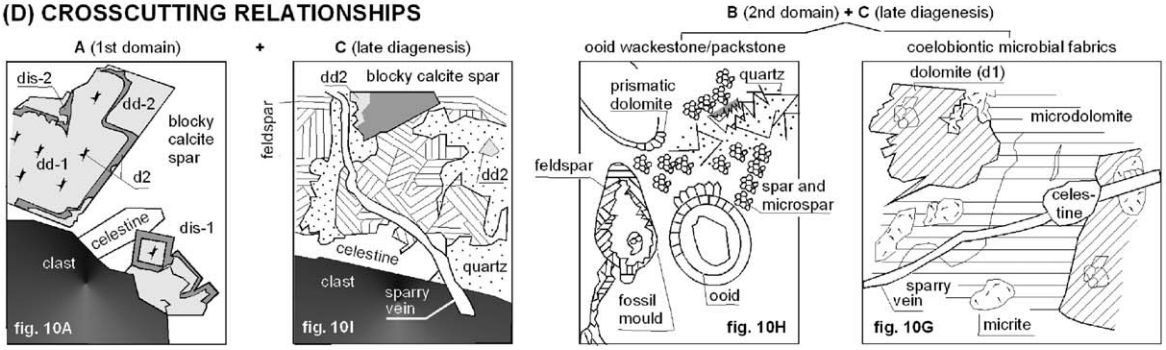

zonation of cements, revealed by cathodoluminescence, allowed correlation of cement zones between samples (Fig. 10A–B). Carbonate content of slope sediments is generally low (<10% in volume) although it increases locally up to 40% in volume. Two carbonate-dominated matrix facies are distinguished in the chaotic megabreccia and breccia sheets. The first facies that filled the intergranular porosity consists of a packstone rich in iron-rich, spastolithic (or plastically deformed) ooids (Fig. 10D–E) and shelly fragments (Fig. 10H), locally bounded by microbially induced clotted textures (Fig. 10C). Ooidal nuclei are commonly rich in iron oxides, and covered by a radiaxal calcitic cortex (Fig. 10D), in some cases surrounded by prismatic rims of calcite crystals (10–15 μm in size). The matrix is composed of microspar to drusy sparite, is iron-rich and contains an important claystone fraction (up to 25% in volume). The second matrix facies consists of microbial thromboids characterized by the presence of clotted textures embedded in a dolomicrosparite (Fig. 10C and G) with homogeneous dull-luminescence under cathodoluminescence. Both early cementation (calcite and iron oxides) and coelobiontic (living in cryptic cavities) microbial activity participated to the stabilization of both the porous walls and the terrigenous material filling the intergranular porosity. A detailed diagenetic study under optical microscope and cathodoluminescence permits the reconstruction of the diagenetic processes affecting the volcaniclastic sediments. A virtual diagenetic sequence is proposed in Fig. 9 involving early-to-late diagenetic processes, in which two diagenetic domains are distinguished.

The first diagenetic domain (Fig. 9A), in which only late-diagenetic cements are preserved, is recognisable in the chaotic megabreccia and breccia sheets of sections JB_{10} and JB_{12} (Fig. 7). The porosity-occluding phases represent, in chronological order, precipitation of celestine, dolomite (in which two stages of dedolomitization are identifiable, respectively replaced by calcite and iron-rich calcite), and calcite cements (Fig. 10A–B). Usually, some of these cementation processes, were preceded and accompanied by solution phenomena as indicated by the presence of embayed contacts and millimetre-sized vugs. Other secondary porosities were induced by fracturing leading to the formation of veins and fissures.

The second diagenetic domain (Fig. 9B) occurs in the heterolithic terrigenous belt of section JB_{11} (Fig. 7). Ca. 45% of the matrix sediment is composed of an ooidal wackestone-to-packstone ironstone. Ooids contain either quartz, feldspar or volcanigenic nuclei (up to 250 μm in size), and a radiaxial cortex of ferroan calcite (Fig. 10D–E). Hematite and chamosite occur impregnating both nuclei and dispersed clasts even at grain contacts. Two kinds of matrix are preserved: microsparite to sparry calcite (Fig. 10D) and microsparite dolomite (Fig. 10E). The first matrix, drusy texturally and 10–50 μm in size, contains dispersed clays and iron-oxide opaques, and has dull luminescence, whereas prismatic crystals (50–75 μm long) coating both ooids and clasts have bright-yellow luminescence and may replace marine fibrous cements related to early burial (Choquette and James, 1987). The second-type fine crystalline dolomitic matrix, commonly observed in microbial thromboids facies, consists of closely packed, euhedral crystals (less than 10 μm in size; Fig. 10G). Both carbonate-dominated matrix facies are characterized by a matrix-supported texture, and display a variable degree of fabric preservation ranging from mimetic (clotted textures and voids) to destructive (unrecognisable mosaics). In the ooidal wackestone-to-packstone facies, the prismatic ooidal rims are locally replaced with mimetic dolomite crystals. The following cement consists of dolomite, calcite (resulting from dedolomitization and late influence of calcite-saturated fluids) and celestine crystals.

The onset of late diagenesis (Fig. 9C) is marked by stylolite-related fracturing and partial dissolution, which crosscut the above-reported two diagenetic domains. At least, six further porosity-occluding cementation phases occur in solution voids and veins. Early dolomite, calcite and celestine cements are locally replaced by feldspar. Particularly, the ooidal-packstone ironstone facies was partly dissolved generating porosities occluded by feldspar and quartz cements. Authigenic feldspars are altered and replaced by fibrous clays, which predate silicification, precipitation of iron oxi-hydroxide crystal cements of pyrite and deerite, and calcite. The onset of late diagenesis

Fig. 10. (A)–(B) Paired transmitted light and cathodoluminescence photomicrographs of JB_{10}: celestine postdated by dolomite replaced by calcite in the dolomite-rhomb core (dedolomitization dd1); a second dedolomitization phase affects the external part of red-luminescent dolomite rhombs; both dedolomitization processes are associated with dissolution as shown by the irregular contacts between red-luminescent dolomite and dull-brown to orange luminescent calcite in rhombs (dis1) and outside (dis2). (C) Microbially induced clotted texture; the porosities between clots are filled by dolomite rhombs. (D) Ooids with radiaxal cortex and ferrugineous-grain nucleus; oolites and clasts rimmed by irregular prismatic calcite fringes (arrowed). (E) Ooidal packstone with ooids and clasts rimmed by prismatic calcite fringes replaced by small dolomite rhombs; matrix composed of fine, dull-reddish luminescent, dolomite rhombs that replaced drusy calcite cement in the intergranular porosity; clast previously covered by an irregular iron-rich crust and rimmed by prismatic calcite fringes. (F) Anhedral dolomite crystals (50–150 μm in size) as xenotopic mosaics and euhedral crystals in contact with cavities. (G) Mimetic microdolomite in thromboid boundstone facies followed by precipitation of anhedral to euhedral replacive dolomite; all diagenetic phases are crosscut by two fracturing phases, one infilled by late calcite crystals rich in iron oxides and a second post-dating characterized by white calcite microcrystals. (H) Intragranular porosity of bivalved skeleton infilled by blocky calcite cements replaced by feldspar on internals wall and associated with veins filled by feldspar cements. (I) Late diagenetic succession affecting both JB_{10} and JB_{11} composed of celestine on the wall clast, dissolved and replaced by a feldspar (f) progressively replaced by quartz (q), and a late fracture filled by bright luminescent, calcite (calc) crosscutting all the previous diagenetic phases. All bar scales = 500 μm, except D where = 250 μm.

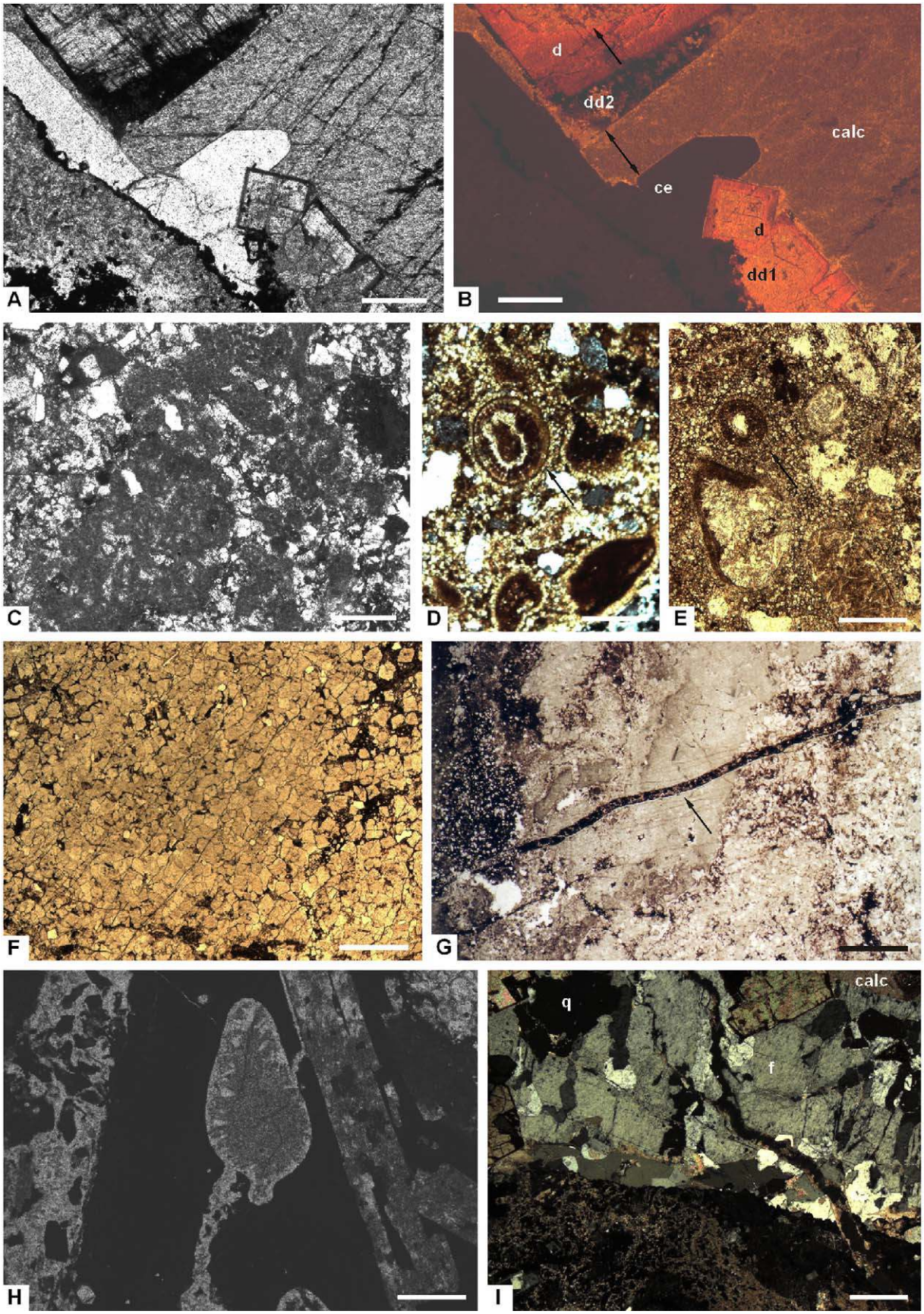
A
B
d
dd2
ce
calc
d
dd1
C
D
E
F
G
H
I
q
f
calc

(Fig. 9C) is marked by stylolite-related fracturing and partial dissolution, which crosscut the above-reported early-diagenetic phases. At least, six further porosity-occluding cementation phases occur in solution voids and veins. Early dolomite, calcite and celestine cements are locally replaced by feldspar. Particularly, the ooidal-packstone ironstone facies was partly dissolved generating porosities occluded by feldspar and quartz cements. Authigenic feldspars are altered and replaced by fibrous clays, which predate silicification, precipitation of iron oxi-hydroxide crystal cements of pyrite and deerite, and calcite.

The presence of active carbonate productivity in the primary porosities of the Boho slope-apron is suggested by widespread development of a robust, coelobiontic (living in cryptic pores), non-skeletal (microbial), carbonate factory (Fig. 10C) that was resilient to poisoning by episodic terrigenous influx. The hematite–chasmolite ooids described on the uppermost Boho flanks originated, most probably, through coating and impregnation and are associated with a peak in carbonate productivity reflecting shallow-water substrates under conditions of low-sediment supply or periodically reduced influx, intense wave-induced rolling, and adequate iron supply from the volcanic rocks. The introduction of ferruginous weathering products would be related to relatively rapid transgression, demise of terrigenous input and subtropical climate (Young and Taylor, 1989; Álvaro et al., 2000), which presumably led to intensified chemical activity. Diagenesis in the slope-apron deposits includes marine, meteoric to deep-burial cementation. Marine diagenesis is restricted to minor micrite envelopes, local cementation and iron-rich matrix (ooidal packstones); a meteoric diagenesis is indicated by development of neomorphic microsparite and dissolution; a deep burial diagenesis is characterized by distinct stages of dolomitization, authigenic feldspar and quartz precipitation. K-feldspar precipitation requires high silica input and high K/H ratios (Morad et al., 2000); its supply is associated with brines, alteration of detrital silicates, particularly feldspars or compaction and pressure solution (Schmid et al., 2004). Finally, as pointed out by Álvaro et al. (2000), deposition of the Adoudou and Lie-de-vin formations was influenced by the establishment of an Early-Cambrian arid subtropical belt on the southern Hemisphere. The record of celestine cements occluding the Boho slope-apron porosity can be related to interstitial precipitation from hypersaline pore-fluids (likely related to the overlying Lie-de-vin strata rich in stromatolites and deposited under common peritidal environments) reflecting distinct fluctuations in salinity.

6. Sedimentary architecture of the clastic wedge

As reported above, the breccia-type, lower slope-apron succession that directly covers the Boho volcano is composed of gravity mass sediments, such as rock fall, gliding and debris-flow deposits, which reflect extensive remobilisation of consolidated sediment from the volcanic flanks. Paleocurrent evidence, immature clast composition, and facies distribution indicate short-distance transport leading to deposition of polyphasic, polymictic breccias. In contrast, the overlying, onlapping-slope heterolithic terrigenous belt shows sporadic evidence of channelized outwash. Its deposition has recorded wave and storm influence both as sandy shoal and shale deposits, whereas conglomeratic lags of channels contain polyphasic, intraformational clasts illustrating cannibalistic processes affecting the slope. Therefore, active erosion of the Boho volcano has not necessarily been a continuous process, as shown by the setting of two major truncation discontinuities recognized at the slope-apron contacts between (i) the chaotic megabreccia and the amalgamated breccia sheets and (ii) the latter and the heterolithic terrigenous belt, and by the presence of unidirectional, isolated and amalgamated channels in the heterolithic terrigenous belt. These sharp changes in sedimentation rate are probably related to abrupt changes in paleorelief sloping and transport mechanism from (i) subaerial (?) rock fall at the foot of the escarpment to sheet-like debris-flow deposition on the slopes, and (ii) the final demise in mass movements replaced by wave- and storm-dominated influence.

The heterolithic terrigenous belt, which occurs onlapping the underlying chaotic megabreccia and amalgamated breccia sheets, can be related to a sequence analysis that evidences relative sea-level fluctuations, as it may be subdivided into composite, large-scale depositional systems. These are composed of lower transgressive (retrogradational) systems tracts (TST), topped by levels of maximum flooding surfaces, and upper highstand (retrogradational) systems tracts (HST) topped by major erosive surfaces: e.g. in the central log (JB_{10}), the heterogeneous terrigenous belt can be subdivided into two composite shallowing-to-deepening-upward trends, both of them topped by purple claystones, which constitute their respective flooding surfaces. Both shallowing trends include an overall thickening- and coarsening-upward trend reflecting progressive shallower conditions and progradation. Their tops are major stratigraphic discontinuities recognized as laterally correlatable erosive contacts (see Fig. 7). As a result of a final flooding of this slope-apron, the episodic fall in siliciclastic input and the subsequent record of claystones under low-energy conditions, an active and episodic carbonate productivity, in the form of microbial mats (stromatolites), took place leading to the typical facies of the Lie-de-vin formation.

The erosion at the top of the Boho volcano is still effected at present by spallation of pervasively jointed blocks, a feature visible both in hand sample and thin section. Joint sets are arranged in a radial framework from the volcanic axe, and tend to be vertical to subvertical. As the slope of the volcano ranges from 50 to 15°, and becomes gentle at the bottom, jointing concentration and steep cliffs diminish downwards, where a smooth lower slope replaces the upper fractured escarpment. As a result, slope blocks on surrounding oueds have a characteristic angular, oblong shape.

7. Conclusions

The volcanic eruptions recorded across the Neoproterozoic-Cambrian transition in the Moroccan Anti-Atlas are still represented by several volcanic cones in the El Graara massif. The Boho volcano (534 ± 10 Ma) of the Alougoum volcanic complex forms a topographic high of ca. 300 m and ellipsoidal transverse outline (ca. 6×22 km). This polygenic stratovolcano expelled explosively eruptive products identifiable in lavas and pyroclastic tuffs. Available petro-geochemical data from the Boho volcano suggest an alkaline magmatism that essentially evolved by fractional crystallization. Continental rift settings usually have geochemical patterns similar to this volcano. An extensional environment, such as continental rifting, fits well the geochemical features of the Boho volcanics.

Subsequent erosion and formation of the Boho slope-apron is characterized by the lack of slumps, olistostromes, and distinct canyons. Rock falls and slides represent the major transport mechanism of consolidated sources. The escarpment morphology supports the assumption that erosion was mainly affected by spallation along subvertical joints. The intense jointing may result from cooling and uncompensated lithostatic pressure exceeding the crushing strength of the volcanic flanks.

In response to the amount of sediment input, the slope-apron underwent phases of inactivity, including reworking. As a result of slope-apron progradation, coarsening- and thickening-upward sequences were sedimented. By contrast, sea-level rise usually lead to reduced sediment supply: consequently, gravity mass movements usually came to an end associated with lowering of gradient slope and transgression, and slope-apron deposits were replaced by normal shoreface-to-offshore sediments. The presence of active carbonate productivity, recorded in the primary porosities of the Boho slope-apron, is suggested by widespread development of a robust, coelobiontic, microbial carbonate factory resilient to poisoning by terrigenous influx.

Acknowledgements

Research of the Alougoum volcanic complex has been supported by ECLIPSE project 'Proterozoic global environmental and climatic changes', and GRICES/CNRST project 'A comparative study of the Neoproterozoic-Cambrian transition between the Portuguese Ossa-Morena Zone and the Moroccan Anti-Atlas and Meseta: geologic and geochemical aspects, and geodynamic model'. The authors thank the peer revision made by Anne Nédelec and an anonymous referee who have greatly improved the ideas explained in the manuscript. This paper is a contribution to IGCP project 485 'Cratons, metacratons and mobile belts: keys from the West African craton boundaries, Eburnian versus Pan-African signature, magmatic, tectonic and metallogenic implications'.

References

Ait Ayad, N., Ribeiro, M.L., Mata, J., Ferreira, P., Ezzouhairi, H., Charif, A., Dias, R., 1998. Evolution du magmatisme cambrien en deux régions périgondwanniennes: Azegour (Haut-Atlas) et Alter do Chao-Elvas (NE Alentejo). Commun. Inst. Geol. Mineiro Portugal 84 (1), B154–B157.

Álvaro, J.J., Rouchy, J.M., Bechstädt, T., Boucot, A., Boyer, F., Debrenne, F., Moreno-Eiris, E., Perejón, A., Vennin, E., 2000. Evaporitic constraints on the southward drifting of the western Gondwana margin during Early Cambrian times. Palaeogeogr., Palaeoclimat., Palaeoecol. 160, 105–122.

Badra, L., Pouclet, A., Prost, A.E., Touray, J.C., 1992. Mise en évidence d'une extension intra-plaque tardi-panafricaine d'intérêt métallogénique dans le Haut Atlas occidental (Maroc). C. R. Acad. Sci. Paris 314, 703–709.

Baker, B.H., Goles, G.G., Leeman, W.P., Lindstrom, M.M., 1977. Geochemistry and petrogenesis of a basalt-benmoreite-trachyte suite from the southern part of the Gregory Rift, Kenya. Contrib. Mineral. Petrol. 64, 303–332.

Boudda, A., Choubert, G., Faure-Muret, A., 1979. Essai de stratigraphie de la couverture sédimentaire de l'Anti-Atlas: Adoudounien—Cambrien inférieur. Notes Mém. Serv. géol. Maroc, 271, 1–96.

Buggisch, W., Flügel, E., 1988. The Precambrian/Cambrian boundary in the Anti-Atlas. Discussion and new results (Morocco). Lect. Notes Earth Sci. 15, 81–90.

Choquette, P.W., James, N.P., 1987. Diagenesis in limestones. 3, the deep burial environment. Geosci. Canada 14, 3–35.

Choubert, G., 1952. Le volcan géorgien de la région d'Alougoum (Anti-Atlas). C. R. Acad. Sci. 234, 350–352.

Choubert, G., 1953a. Histoire géologique du domaine de l'Anti-Atlas. Notes Mém. Serv. géol. Maroc 100, 1–77.

Choubert, G., 1953b. Le Précambrien III et le Géorgien de l'Anti-Atlas. Notes Mém. Serv. géol. Maroc 103, 7–39.

Choubert, G., Faure-Muret, A., 1970. Livret-guide de l'excursion " Anti-Atlas occidental et central " du Colloque international sur les corrélations du Précambrien. Notes Mém. Serv. géol. Maroc 229, 1–259.

Clauer, N., Caby, R., Jeanette, D., Trompette, R., 1982. Geochronology of sedimentary and metasedimentary rocks of the West African Craton. Prec. Res. 18, 53–71.

Compston, W., Williams, J.L., Kirschvink, J.L., Zhang, Z., Ma, G., 1992. Zircon U–Pb ages for the Early Cambrian time scale. J. Geol. Soc. London 127, 319–332.

Debrenne, F., Debrenne, M., 1995. Archaeocyaths of the Lower Cambrian of Morocco. Beringeria Spec. (2), 121–145.

Destombes, J., Hollard, H., Willefert, S., 1985. Lower Palaeozoic rocks of Morocco. In: Hollard, C.H. (Ed.), Lower Palaeozoic rocks of the world, Lower Palaeozoic of North-Western and West Central Africa, vol. 4. John Wiley and Sons, Chichester, pp. 157–184.

Ducrot, J., Lancelot, J.R., 1977. Problème de la limite Précambrien-Cambrien: étude radiochronologique par la méthode U/Pb sur zircon du volcan du Jbel Boho. Can. J. Earth Sci. 14, 1771–1777.

Einsele, G., 1991. Submarine mass flow deposits and turbidites. In: Einsele, G., Ricken, W., Seilacher, A. (Eds.), Cycles and Events in Stratigraphy. Springer-Verlag, Heidelberg, pp. 313–339.

El Archi, A., El Houicha, M., Jouhari, A., Bouabdelli, M., 2004. Is the Cambrian basin of the western High Atlas (Morocco) related either to a subduction zone of a major shear zone? J. African Earth Sci. 39, 311–318.

El Attari, A., 2001. Etude lithostratigraphique et tectonique des terrains cambro-ordoviciens du Môle côtier (Meseta occidentale, Maroc). Ph.D, Rabat University, 394pp.

Ezzouhairi H., 2001. Le magmatisme post-collisionnel panafricain (tardi à post-orogénique) des régions d'Aghbalou, Sidi Flah-Bouskour et Oued Imini (Ouarzazate, Anti Atlas central, Maroc). Lithostratigraphie, géochimie, pétrogenèse et contexte géodynamique. Thèse de Doct. d'Etat, Univ. Chouaïb Doukkali, El Jadida, 201pp.

Ezzouhairi, H., Ribeiro, M.L., Charif, A., Ait Ayad, N., Ramos, F., Moreira, M.E., Coke, C., 2003. Contribution à la caractérisation pétrographique et géochimique du volcanisme cambrien moyen du môle côtier (Maroc). 3ème Colloque International 3MA, Casablanca, 8–10 Mai, livre des résumés, pp. 49–50.

Gawthorpe, R.L., 1987. Burial dolomitization and porosity development in a mixed carbonate-clastic sequence: an example from the Bowland Basin, Northern England. Sedimentology 34, 533–558.

Geyer, G., Landing, E., Heldmaier, W., 1995. Faunas and depositional environments of the Cambrian of the Moroccan Atlas region. Beringeria, Spec. 44 (2), 47–120.

Houzay, J.P., 1979. Empreintes attribuables à des méduses dans la série de base de l'Adoudounien (Précambrien terminal de l'Anti-Atlas, Maroc). Géol. Méditerr. 6, 379–384.

Jouhari, A., El Archi, A., Aarab, M., El Attari, A., Emnih, N., Laduron, D., 2001. Géochimie et cadre géodynamique du volcanisme néoprotérozoïque terminal (Vendien) du Haut Atlas occidental, Maroc. J. African Earth Sci. 32, 695–705.

Kastner, M., 1971. Authigenic feldspars in carbonate rocks. Amer. Miner. 56, 1403–1442.

Kirshvink, J.L., Magaritz, M., Ripperdan, R.L., Zhuravlev, A.Yu., 1991. The Precambrian/Cambrian boundary: magnetostratigraphy and carbon isotopes resolve correlation problems between Siberia, Morocco, and South China. GSA Today 1, 69–71.

Kuno, H., 1966. Lateral variation of basalt magma types across continental margins and island arcs. Bull. Volcanol. 29, 195–222.

Landing, E., Bowring, S.A., Davidek, K.L., Wetrop, S.R., Geyer, G., Heldmaier, W., 1998. Duration of the Early Cambrian: U–Pb ages of volcanic ashes from Avalon and Gondwana. Can. J. Earth Sci. 35, 329–338.

Latham, A., Riding, R., 1990. Fossil evidence of the location of the Precambrian/Cambrian boundary in Morocco. Nature 344, 752–754.

LeBas, M.J., Le Maitre, R.W., Streckeisen, A., Zanettin, B., 1986. A chemical classification of volcanic rocks based on the total alkali silica diagram. J. Petrol. 27, 745–750.

Leblanc, M., 1973. Les formations infracambriennes de Bou—Azzer (Anti Atlas central, Maroc): lithostratigraphie, tectonique et position structurale. Notes Mém. Serv. géol. Maroc 254, 7–14.

Leblanc, M., Lancelot, J.R., 1980. Interprétation géodynamique du domaine panafricain (Précambrien terminal) de l'Anti-Atlas (Maroc) à partir de données géologiques et géochronologiques. Can. J. Earth Sci. 17, 142–155.

Magaritz, M., Kirshvink, J.L., Latham, A.J., Zhuravlev, A.Yu., Rozanov, A.Yu., 1991. Precambrian/Cambrian boundary problem: carbon isotope correlations for Vendian and Tommotian time between Siberia and Morocco. Geology 19, 847–850.

Mata, J., Munha, J., 1990. Magmatogénese de metavulcanitos Câmbricos do nordeste alentejano: os estadios iniciais de ≪ rifting ≫ continental. Commun. Serv. Geol. Portugal 76, 61–89.

Mifdal, A., Peucat, J.J., 1985. Datations U–Pb et Rb–Sr du volcanisme acide de l'Anti-Atlas marocain et du socle sous-jacent dans la région de Ouarzazate. Apport au problème de la limite Précambrien-Cambrien. Sci. Geol. Bull., Strasbourg 38 (2), 185–200.

Monninger, W., 1979. The section of Tiout (Precambrian/Cambrian boundary beds, Anti-Atlas, Morocco): an environmental model. Arb. Paläont. Inst. Würzburg 1, 1–289.

Morad, S., Ketzer, J.M., De Ros, F., 2000. Spatial and temporal distribution of diagenetic alterations in siliciclastic rocks: implications for mass transfer in sedimentary basins. Sedimentology 47, 95–120.

Narbonne, G.M., Landing, E., Anderson, M.M., 1987. A candidate stratotype for the Precambrian–Cambrian boundary, Fortune Head, Burin Peninsula, southeastern Newfoundland. Can. J. Earth Sci. 24, 1277–1293.

Ouali, H., Briand, B., Bouchardon, J.L., El Maâtaoui, M., 2000. Mise en évidence d'un volcanisme alcalin intraplaque d'âge Acadien dans la Meseta nord-occidentale (Maroc). C. R. Acad. Sci. Paris 330, 611–616.

Ouali, H., Briand, B., Bouchardon, J.L., Capiez, P., 2003. Le volcanisme cambrien du Maroc central: implications géodynamiques. C. R. Géosciences 335, 425–433.

Ouazzani, H., 2001. Le volcanisme d'arc massif ancien du Haut Atlas occidental (Maroc), un témoin de la convergence de la branche occidentale de l'océan panafricain. Bull. Soc. géol. France 172, 587–829.

Piqué, A., Bouabdelli, M., Darboux, J.R., 1995. Le rift cambrien du Maroc occidental. C. R. Acad. Sci. Paris 320, 1017–1024.

Radke, B.M., Mathis, R.L., 1980. On the formation and occurrence of saddle dolomite. J. Sedim. Petrol. 50, 1149–1168.

Ribeiro, M.L., 1987. Petrogenesis of early Palaeozoic peralkaline rhyolites from the Macedo de Cavaleiros region (NE Portugal). Geol. Runds. 76, 147–168.

Ribeiro, M.L., Solá, A.R., Moreira, M.E., Ntarmouchant, A., Ramos, J.M.F.M., Ben Abbou, M., Ezzouhairi, H., Charif, A., Dahire, M., 2001. Evolution magmatique péri-gondwanienne au passage Infracambrien-Cambrien: Exemple des magmatites de Bou Ibenrhar-Jbel Hadid (Massif hercynien central, Maroc). Comun. Inst. Geol. Mineiro 88, 245–254.

Schmid, S., Worden, R.H., Fisher, Q.J., 2004. Diagenesis and reservoir quality of the sherwood sandstone (Triassic), Corrid Field, Slyne Basin, West of Ireland. Mar. Petrol. Geol. 21, 299–315.

Schmitt, M., 1979. The section of Tiout (Precambrian/Cambrian boundary beds, Anti-Atlas, Morocco): stromatolites and their biostratigraphy. Arb. Paläont. Inst. Würzburg 2, 1–188.

Sdzuy, K., 1978. The Precambrian–Cambrian boundary beds in Morocco (preliminary report). Geol. Mag. 115, 83–94.

SGM (Service Géologique du Maroc), 1970. Carte géologique de l'Anti-Atlas central et de la zone synclinale de Ouarzazate. Feuilles Ouarzazate, Alougoum et Telouet Sud, 1/200 000. Eds. Service géol. Maroc, Notes et Mém. no. 138.

Soulaimani, A., Bouabdelli, M., Piqué, A., 2003. L'extension continentale au Néoprotérozoïque supérieur-Cambrien inférieur dans l'Anti-Atlas (Maroc). Bull. Soc. Géol. France 174 (1), 83–92.

Sun, S.S., McDonough, W.F., 1989. Chemical and isotopic systematics of oceanic basalts: implications for mantle composition and processes. In: Saunders A.D., Norry M.J. (Eds.), Magmatism in the Oceanic Basins. Geol. Soc. London, Spec. Publ. 42, 313–345.

Spizharski, T.N., Zhuravleva, I.T., Repina, L.N., Rozanov, A.Yu., Tchernysheva, N.Ye, Ergaliev, G.H., 1986. The stage scale of the Cambrian system. Geol. Mag. 123, 387–392.

Tucker, E., 1986. Carbon isotope excursions in Precambrian/Cambrian boundary beds, Morocco. Nature 319, 48–50.

Valladares, M.I., 1995. Siliciclastic-carbonate slope apron in an immature tensional margin (Upper Precambrian–Lower Cambrian), Central Iberian Zone, Salamanca, Spain. Sedim. Geol. 94, 165–186.

Walsh, G.J., Aleinikoff, J.N., Benziane, F., Yazidi, A., Armstrong, T.R., 2002. U–Pb zircon geochronology of the Paleoproterozoic Tagragra de Tata inlier and its Neoproterozoic cover, western Anti-Atlas, Morocco. Precambrian Res. 117, 1–20.

Young, T.P., Taylor, W.E.G. (Eds.), 1989. Phanerozoic Ironstones. Geol. Soc. London, Spec. Publ., vol. 46.

Zenger, D.H., 1983. Burial dolomitization in the lost Burro Formation (Devonian), east-central California, and the significance of late diagenetic dolomitization. Geology 11, 519–522.